Contrast decay in a trapped-atom interferometer

A. Hilico, C. Solaro, M.-K. Zhou, M. Lopez, and F. Pereira dos Santos*

LNE-SYRTE, Observatoire de Paris, PSL Research University, CNRS, Sorbonne Universités, UPMC Univ. Paris 06,
61 avenue de l'Observatoire, 75014 Paris, France

A Ramsey-Raman interferometer is used to realize a compact force sensor using cold ^{87}Rb atoms trapped in a vertical optical lattice. The sensitivity and accuracy of the force measurements are discussed and the limits in short-term sensitivity evaluated. We reach a relative sensitivity on the Bloch frequency and thus on the gravity acceleration of 3.9×10^{-6} at 1 s. We perform an experimental study of the influence of the transverse confinement onto the decay of the interferometer contrast and compare the measurements with a simple semiclassical model. It is shown that vertical gradients of the trapping potential can contribute significantly to the loss of contrast.

　　　　　PACS number(s): 37.25.+k, 32.80.Qk, 37.10.Jk, 05.60.Gg

Inertial sensors based on atom interferometry now reach impressive sensitivities and accuracies, giving rise to new applications in high-precision measurements, particularly gravimeters [1–4], gradiometers [5,6], gyrometers [7–10], and velocity sensors for the measurement of photon recoil and the determination of the fine structure constant [11]. The performances of these atomic interferometers (AI) are competitive with other devices based on other technologies, e.g., optical interferometers [4]. Yet, in most cases, these apparatus remain complex, bulky, and hardly movable. The size of these instruments, when using free falling atoms, scales quadratically with the interferometer time and so does the intrinsic sensitivity. Various miniaturization schemes are currently investigated, with efforts towards simplification [12–15] and in engineering of subsystems [16–18]. As an alternative, the falling distance can be reduced using either semitrapped configurations, based, for instance, on the use of Bloch oscillations to levitate the atoms [19,20], or trapped geometries such as those based on atom chips [21–23] or optical lattices [24,25].

In this paper, we report the characterization of an atomic sensor based on ^{87}Rb atoms trapped in a shallow vertical optical lattice. A so-called Ramsey-Raman interferometer allows for the precise measurement of the energy difference between neighboring lattice sites. After a short review of the measurement principle, we present the performances of our second generation setup in terms of sensitivity and accuracy. Finally, we investigate the influence of the trapping laser's parameters onto the contrast decay.

I. PRINCIPLE OF THE EXPERIMENT

In our system, we consider laser-cooled ^{87}Rb atoms trapped in a vertical one-dimensional (1D) lattice far detuned from resonance. Atoms experience a periodic potential $\hat{H}_l = U_l[1 - \cos(2k_l\hat{z})]/2$, which adds to the gravitational potential $\hat{H}_g = m_a g\hat{z}$ and to kinetic energy represented by $\hat{H}_k = \frac{p^2}{2m_a}$. U_l and k_l represent the lattice depth and wave number, m_a is the atomic mass, and g the gravity acceleration. Restricting the problem to the fundamental Bloch band, the eigenstates of the total

Hamiltonian $\hat{H}_{\text{tot}} = \hat{H}_k + \hat{H}_l + \hat{H}_g$ are given by the Wannier-Stark (WS) states $|W_m\rangle$ [26], where the quantum number m is the well index which labels the different lattice sites. The increment of energy between two consecutive states is equal to

$$h \times \nu_B = m_a g\lambda_l/2, \tag{1}$$

where $\nu_B \sim 568.5$ Hz is the Bloch frequency and λ_l is the wavelength of the lattice laser. Considering the two internal hyperfine states $|g\rangle = |5\,^2S_{1/2}, F = 1, m_F = 0\rangle$ and $|e\rangle = |5\,^2S_{1/2}, F = 2, m_F = 0\rangle$, one obtains two WS ladders separated by the $h \times \nu_{\text{HFS}}$, where $\nu_{\text{HFS}} \sim 6.834$ GHz is the hyperfine structure frequency (HFS). The corresponding two sets of eigenstates $|g, W_m\rangle$ and $|e, W_m\rangle$ are shown in Fig. 1.

The spread of the atomic wave function depends on the lattice depth [28]. For shallow depths ($U_l < 5E_r$, where $E_r = \hbar^2 k_l^2/2m_a$ is the recoil energy of a lattice photon) the wave function extends across a significant number of wells [27,28]. This delocalization allows for resonant tunneling between different lattice sites using coherently driven two-photon stimulated transition with counterpropagating vertical Raman beams [29]. Rabi oscillations between $|g, W_m\rangle$ and $|e, W_{m'}\rangle$ can be induced either in the same well ($m = m'$) or in neighboring wells ($m \neq m'$). By energy conservation, such a transition occurs when the frequency difference of the two Raman beams fulfils $\nu_{R1} - \nu_{R2} = \nu_{\text{HFS}} + \Delta m \times \nu_B$ (where $\Delta m = m - m'$). This resonance yields the value of ν_B.

In this system, we have demonstrated sub-Hz spectroscopy of WS states and various types of AI [24,30], allowing for the measurement of ν_B with a relative sensitivity of 9×10^{-6} at 1 s at best. Using Rabi frequencies larger than ν_B, multiwave interferometers have also been realized [31]. All these measurements were limited by the detection noise.

To overcome this limitation, the experimental setup has been upgraded, improving mainly the number of trapped atoms and the detection efficiency. We first realize in a new vacuum chamber a three-dimensional (3D) magneto-optical trap (MOT) at a base pressure of 10^{-10} mbar, resulting in a lifetime of 40 s. About 10^8 atoms are collected in 500 ms and cooled to 2 μK in a –20 Γ detuned molasses phase. The atoms are then optically pumped into $|5\,^2S_{1/2}, F = 1, m_F = 0\rangle$ state to reduce the influence from stray magnetic fields. The lattice is created by a vertically retroreflected and single-mode
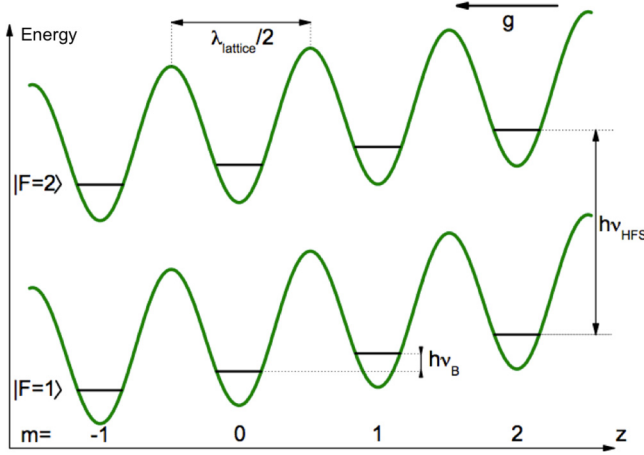

FIG. 1. (Color online) Wannier-Stark ladders of states. The two internal states are separated by the hyperfine transition frequency ν_{HFS}. The increment of energy between neighboring wells corresponds to the increment of gravitational potential energy $h \times \nu_B$, where ν_B is the Bloch frequency.

frequency-doubled Nd : YVO$_4$ laser ($\lambda_l = 532$ nm, $P = 7.5$ W, and $1/e^2$ radius of ~ 1 mm), leading to a lattice depth of $\sim 1.7 E_r$. This depth can be increased up to 3.9 E_R by changing the waist of the laser. Transverse confinement is provided by an additional red detuned progressive wave from a Yb fiber laser ($\lambda = 1064$ nm, $0.3 < P_{\mathrm{IR}} < 2$ W, and $1/e^2$ radius of 145 μm on the atoms) aligned along the lattice axis. This infrared (IR) trap induces a large differential light shift (DLS) on the hyperfine states (~ 3.3 Hz/W). An anti-light-shift (ALS) beam well mode-matched is superimposed on this IR laser. To produce the ALS beam, we use a few nanowatts from a laser red detuned from the D2 transition of 3 GHz. This laser creates a DLS of opposite sign, which compensates for the IR DLS and its inhomogeneities [24]. Finally, around 75 000 atoms are distributed in a 1-mm-long cloud (about 4000 adjacent WS states) in the fundamental lattice band. The lifetime of the atoms in the mixed trap is ~ 7 s. This represents an improvement of about 1 order of magnitude both in the atom number and in their lifetime in the trap compared to the previous setup [24,30].

The atoms are interrogated using counterpropagating circularly polarized Raman beams which are carefully aligned onto the lattice. With respect to our previous work [30], Raman detuning has been increased from 3 to 300 GHz from the ^{87}Rb D2 line, enabling the impact of the Raman DLS to decrease by 1 order of magnitude. The maximal total Raman power is ~ 10 mW distributed over a $1/e^2$ radius of ~ 2.6 mm. This leads to a maximum Rabi frequency of 25 Hz for a transition $\Delta m = 7$ at a depth of 1.6 E_R. Typical interrogation time is around 1 s. The Raman transition changing both the internal and external states, we use a state-selective detection based on a time-of-flight fluorescence. From the measurement of the populations in the two hyperfine states N_g and N_e we compute the transition probability from $|g\rangle$ to $|e\rangle$: $P_e = \frac{N_e}{N_g + N_e}$. The optical system collecting the fluorescence has been changed from a system collecting 1% of the fluorescence with a single photodiode to a symmetrical one collecting 8.6% on two
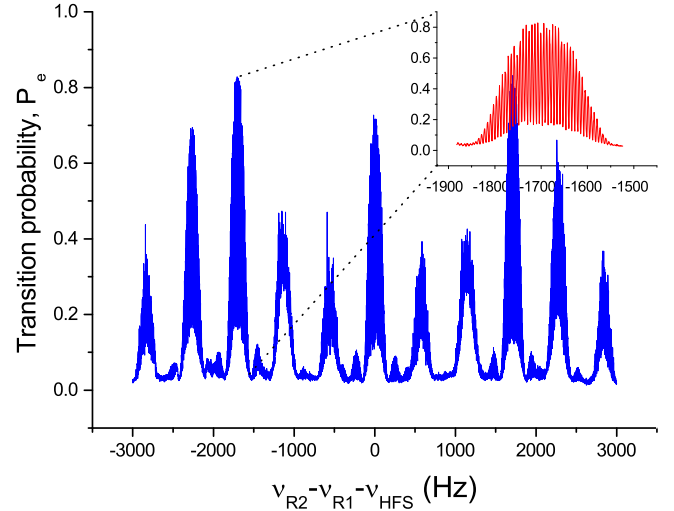

FIG. 2. (Color online) Ramsey-Raman fringes for a lattice depth $U_l = 3.9 E_r$ showing evidence of transitions between up to five neighboring lattice sites. Rabi envelopes are separated by the Bloch frequency $\nu_B \sim 568.5$ Hz and contain interference fringes with an interfringe of $\Delta\nu = 1/T_R$. Here $\tau_{\pi/2} = 10$ ms and $T_R = 150$ ms. The intensities of the Raman lasers and the lattice depth were set to optimize the contrast of the $\Delta m = \pm 3$ fringes. Insert: zoom on the $\Delta m = -3$ transition.

independent photodiodes. With respect to our previous results, we are now dominated by the contribution from quantum projection noise. Combined with the increased number of atoms, it enables us to reduce the detection noise by a factor of 10.

II. SENSITIVITY MEASUREMENT

We report here the measurement of ν_B using an interferometer scheme called a Ramsey-Raman interferometer [24]. This interferometer is composed of two $\pi/2$ pulses of duration $\tau_{\pi/2}$ separated by a free precession time T_R. During this AI, the atomic wave functions are placed in a coherent superposition of two wave packets centered in two different wells. A fringe pattern such as displayed in Fig. 2 is obtained by scanning the frequency difference between the two Raman $\nu_{R1} - \nu_{R2}$ around the HFS frequency. We observe sets of Ramsey fringes in each Rabi envelope corresponding to a given Δm transition. The fringe spacing is $\sim 1/T_R$.

We report here on our best sensitivity measurement realized using a transition $\Delta m = \pm 7$ at a depth $U_l = 1.7$ E_r, with $T_R = 900$ ms and $\tau_{\pi/2} = 10$ ms with a fringe contrast of about 20%. To determine the sensitivity of our measurement, we localize and monitor the fluctuations of the position of the central fringes of our interferometers (displayed in Fig. 3) using the integration scheme described in Ref. [30]. The long-term frequency fluctuations of the $+$ and -7 ν_B measurements are dominated by a frequency shift of the clock transition ν_{HFS} due to polarization fluctuations in the ALS fiber inducing slow light-shift fluctuations. Computing the half difference of the frequency fluctuations of the two $\Delta m = +7$ and -7 interferometers enables us to get rid of this effect and to recover the intrinsic ν_B fluctuations.
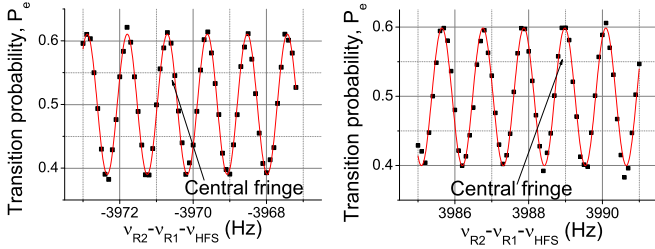
FIG. 3. (Color online) Ramsey-Raman fringes around -7 and $+7$ ν_B for a lattice depth of $U_l = 1.7$ E_r with $T_R = 900$ ms and $\tau_{\pi/2} = 10$ ms. The central fringe of the interferometers is indicated and the red curve is a sinusoidal fit.

To quantify our sensitivity, we compute the Allan standard deviation of this half difference, displayed in Fig. 4. We obtain a relative short-term sensitivity corresponding to $\frac{\sigma_\nu}{7\nu_B} = 3.9 \times 10^{-6}$ at 1 s. As the short term frequency fluctuations are filtered by the digital integrator locking the Raman frequency difference onto the central fringes, we extrapolate the sensitivity to 1 s, assuming the noise to be white and averaging as $1/\sqrt{T_{\mathrm{meas}}}$ where T_{meas} is the measurement time. The sensitivity decays as a white noise down to 1.5 mHz in 200 s and increases for larger measurement times due to residual frequency fluctuations.

III. NOISE BUDGET

Remarkably, we repeatedly obtain about the same relative sensitivity of $\sim 5 \times 10^{-6}$ at 1 s with other sets of parameters and other interrogation schemes (Rabi spectroscopy or symmetric interferometers [30]). To understand this limit, a noise budget was performed, determining the contributions of the different sources of noise: detection noise, trapping lasers noise, Raman laser noise, and vibration noise.
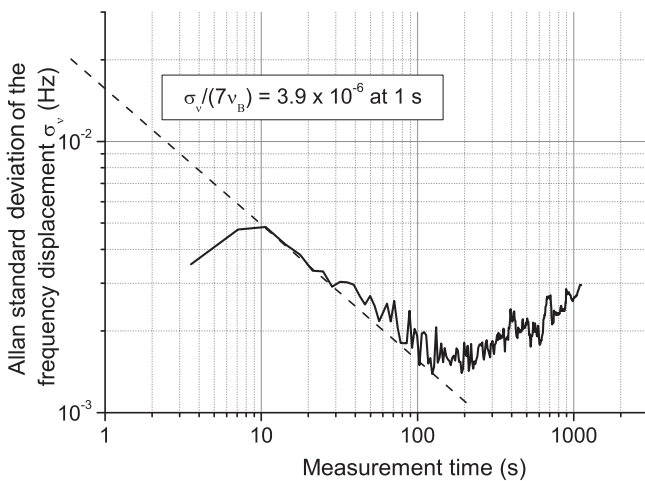

FIG. 4. Allan standard deviation of the half difference of the frequency fluctuations of $\Delta m = +7$ and -7 transition measured with a Ramsey-Raman interferometer with experimental parameters $\tau_{\pi/2} = 10$ ms and $T_R = 900$ ms. The half difference cancels the hyperfine transition fluctuations and decays in $1/\sqrt{T_{\mathrm{meas}}}$. The black dashed line is a guide to the eyes.

TABLE I. Noise budget.

Noise	σ_ν at 1 s	$\frac{\sigma_{\delta\nu}}{7 \times \nu_B}$
Trapping lasers noise	13 mHz	3.25×10^{-6}
Raman lasers noise	7 mHz	1.76×10^{-6}
Detection noise for $C = 20\%$	5.9 mHz	1.9×10^{-6}
Vibration noise for $\Delta m = 7$	11.2 mHz	2.8×10^{-6}
Sum	21.9 mHz	$\sim 5.5 \times 10^{-6}$

Using a 0.5-ms-long $\pi/2$ microwave (MW) pulse, we measure the noise on the transition probability due to detection noise: $\sigma_{Pe} = 3.3 \times 10^{-3}$ at 1 s. We deduce the impact of the detection noise onto the frequency noise of the interferometer using

$$\sigma_\nu = \frac{\sigma_{P_e}}{C\pi T_R}. \qquad (2)$$

For a contrast $C = 20\%$ and $T_R = 900$ ms, we find $\sigma_{\nu,\mathrm{det}} \sim 5.9$ mHz. Using a MW Ramsey interferometer of 80% contrast for $T_R = 900$ ms and $\tau_{\pi/2} = 10$ ms, we measure the noise due to the trapping lasers. We find $\sigma_{Pe} = 2.9 \times 10^{-2}$ at 1 s, which corresponds to a frequency noise $\sigma_{\nu,\mathrm{lasers}} = 13$ mHz. By shining the Raman lasers (off resonance with respect to the two-photon transition) during the MW pulses, we deduce an additional noise contribution $\sigma_{\nu,\mathrm{Raman}} = 7$ mHz at 1 s, which we attribute to the Raman DLS fluctuations. Finally, the contribution of the mirror vibration noise is determined from the measurement of a seismometer, whose velocity signal is weighted by the transfer function of our Ramsey-Raman interferometer. For $\Delta m = \pm 7$ we calculate $\sigma_{\nu,\mathrm{vib}} = 11.2$ mHz at 1 s, which corresponds to an acceleration noise of 2.8×10^{-6} g at 1 s, due to ground vibration noise.

Adding up all these noise contributions summarized in Table I, we obtain a total frequency noise $\sigma_{\nu,\mathrm{tot}} = 19.4$ mHz at 1 s, yielding a relative sensitivity on the Bloch frequency for a measurement of the $\Delta m = 7$ transition of $\frac{\sigma_{\nu,\mathrm{tot}}}{7\nu_B} = 4.8 \times 10^{-6}$ at 1 s. This short-term sensitivity corresponds to the one we obtain routinely. The trapping laser noise is slightly predominant, though the intensities of all trapping lasers are locked. This noise may come from fluctuations of the differential light shifts seen by the atoms due to laser-pointing fluctuations.

IV. ACCURACY STUDY

The Bloch frequency depends on three quantities that can be determined independently with high accuracy: the wavelength of the lattice laser λ_l, the h/m_a ratio and g. The lattice laser is locked on an iodine line using a frequency modulation transfer spectroscopy (hyperfine transition $a1$ of the 1116/P(52)32-0 line at 532.195951(03) nm [32]). We estimate the relative uncertainty on λ_l to be about 2×10^{-9}, h/m_a is known to one part in 10^9 [11]. Gravity acceleration g has been measured in the laboratory room by atomic and conventional corner-cube gravimeters. From these values, we compute the expected value of the Bloch frequency: $\nu_{B,\mathrm{expt}} = 568.509003(6)$ Hz. It differs from our mean measurement $\nu_{B,\mathrm{meas}} = 568.542(4)$ Hz for an IR laser power of 0.5 W. This corresponds to a well resolved relative difference of 5×10^{-5}. The measured value
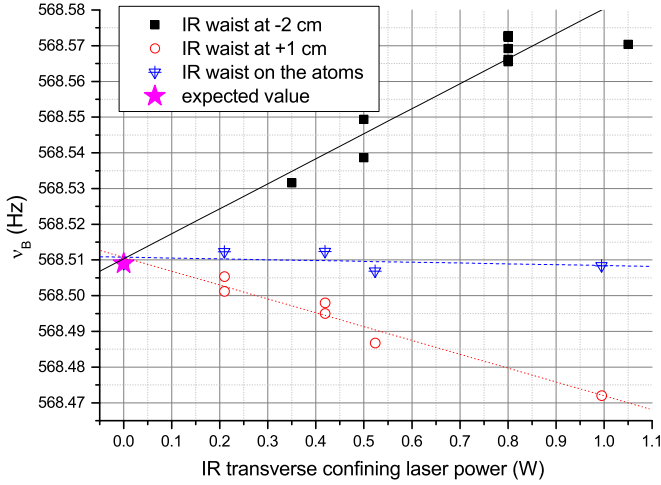
FIG. 5. (Color online) Measurement of the Bloch frequency ν_B versus the IR transverse trap laser power for different IR waist positions. Black squares: waist 2 cm below the atoms. Red circles: 1 cm above. Blue triangles on the atoms. The corresponding curves are linear fits. The measurements have been realized for interferometers at $\Delta m = \pm 7$ and ± 6 transitions at $U_l \sim 1.8\ E_R$. The pink star represents the expected value $\nu_{B,\text{expt}}$.

corresponding to an acceleration larger than g, the difference cannot be due to an error of the lattice tilt. Moreover, we estimate our uncertainty on verticality to be 0.5 mrad leading to a relative uncertainty of $\sim 10^{-7}$.

We studied the impact of the IR laser power (P_{IR}) on the measurement of ν_B, depicted by the black squares of Fig. 5. We observed a fairly linear dependence versus the IR power. A linear fit to the data gives $\nu_{B,\text{meas}} = \nu_{B_0} + \beta \times P_{\text{IR}}$ with $\beta = 69.9\ (7)$ mHz/W and $\nu_{B_0} = 568.510\ 3(50)$ Hz. The extrapolation at 0 power ν_{B_0} is close to the expected value.

We attribute this effect to a residual dipole force which occurs if the atoms are not at the waist of the IR beam. To estimate this effect, we consider the dependence of the IR laser intensity on z. The on-axis intensity is given by

$$I_{\text{IR}}(P_{\text{IR}}, z) = \frac{2 P_{\text{IR}}}{\pi\, w_{\text{IR}}^2} \left(\frac{w_{\text{IR}}}{w_{\text{IR}}(z)} \right), \tag{3}$$

where $w_{\text{IR}}(z)$ is the $1/e^2$ radius of the IR laser and $w_{\text{IR}} = w_{\text{IR}}(z = 0) = 145\ \mu$m is the waist radius. The trap depth $U_{\text{IR}}(z, P_{\text{IR}})$ being proportional to I_{IR}, atoms that are not at the laser waist feel slightly different potentials while tunneling from Δm wells. This creates a frequency offset, proportional to the IR power:

$$\Delta \nu_{\text{IR}}(P_{\text{IR}}, z, \Delta m)$$
$$= \frac{U_{\text{IR}}(P_{\text{IR}}, z + \Delta m \times \lambda_{532}/2) - U_{\text{IR}}(P_{\text{IR}}, z)}{\Delta m \times h}. \tag{4}$$

Computing this effect versus P_{IR} and using z as a free parameter, we find that the black squares of Fig. 5 correspond to a waist ~ 2 cm below the atoms, which is comparable to the Rayleigh length but significantly larger than the expected positioning uncertainty of a few mm.

We then performed similar measurements at other positions of the waist with respect to the atoms. The beam waist was

displaced in a controlled way by translating the 400 mm focal length lens that focuses the transverse beam. The results are represented by the red circles and blue triangles of Fig. 5. We observe again linear behaviors, with different slopes, corresponding to a waist positions located approximately 1 cm above and on the atoms. The three extrapolated frequencies at $P_{\text{IR}} = 0$ W match with each other and are in a good agreement with the theoretical prediction.

V. CONTRAST DECAY STUDY

A. Systematic study

We performed a study of the contrast decay of our interferometers versus the free precession time T_R, depending on the separation Δm and the lattice depth U_l. For each measurement, we tuned the lattice depth in order to be at a local maximum of coupling for a given Δm transition [33]. Typical measurements for a waist-atom distance $z = -2$ cm are displayed in Fig. 6. Contrasts decay exponentially, faster when the depth is higher and the separation bigger. For comparison, we measured the contrast decay of a microwave Ramsey interferometer (black squares), which decreases much more slowly with T_R, keeping a contrast as large as 80% for $T_R = 1.8$ s. Fitting the decays with $C_0 \times e^{-\gamma T_R}$, depicted by the black dashed curves of Fig. 6, we observe decay rates γ ranging from 0.8 to 1.6/s for various separations and depths. We do not observe a clear correlation between decay rates and separations or depth, but for these measurements separation and depth are linked, as optimizing the coupling for a given separation requires one to adjust the lattice depth. On the other hand, the dependence of coupling versus the depth exhibits for some separations several maxima. This allows one to perform measurements for the same separation $\Delta m = 3$ at two different
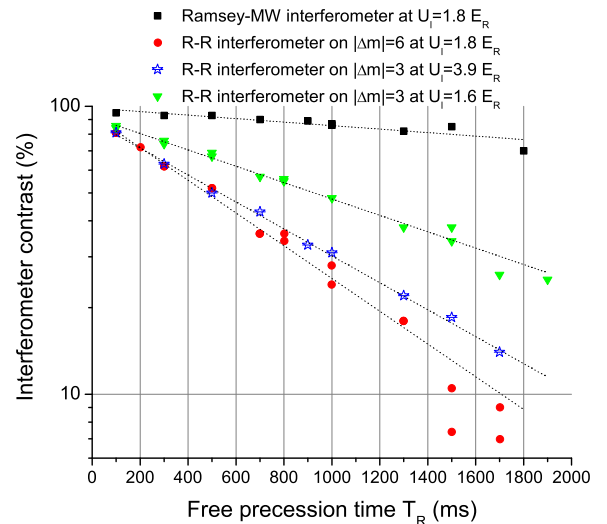

FIG. 6. (Color online) Ramsey-Raman interferometer contrast versus T_R in semilog scale. Red circles correspond to $\Delta m = +6$ and –6 transitions at $U_l = 1.8\ E_R$, green triangles correspond to $\Delta m = +3$ transition at $U_l = 1.6\ E_R$, and blue diamonds correspond to $\Delta m = +3$ transition at $U_l = 3.9\ E_R$. Black squares correspond to the contrast of a Ramsey-MW interferometer. All measurements were performed at $P_{\text{IR}} = 0.5$ W, and at $z = -2$ cm. Black dashed curves correspond to exponential decay fits to the data.
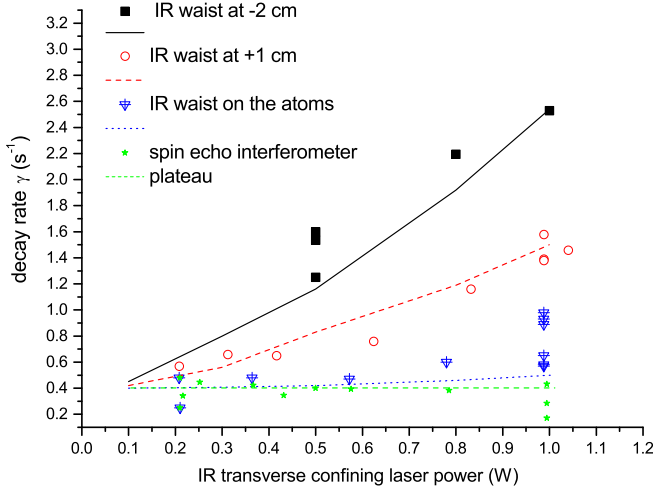
FIG. 7. (Color online) Ramsey-Raman interferometer contrast decay measurements and calculations versus P_{IR} for different IR waist-atoms distances. Measurements have been performed for $\Delta m = +6$ and -6 transitions at $U_l \sim 1.8\ E_R$. Black squares correspond to a IR waist-atoms distance of -2 cm, red circles $+1$ cm, and for the blue triangles the waist is approximately on the atoms. Green stars correspond to a spin-echo interferometer with the IR waist on the atoms. The green dashed line represents the plateau at 0.4/s. The black, red, and blue curves correspond to decay rate calculations using the model explained in Sec. V B for a waist-atoms distance of, respectively, $z = -2, +1$, and $+0.2$ cm and a waist of 145 μm.

depths 1.6 and 3.9 E_R [33]. The decay rate at 3.9 E_R is twice bigger than at 1.6 E_R.

We also performed a contrast decay study for various P_{IR} and IR waist positions at a given depth $\sim 1.8 E_R$ on the $\Delta m = 6$ transition. For these measurements we used a symmetrical Ramsey interferometer, adding two MW π pulses as for the accordion interferometer described in Ref. [30]. This configuration makes the interferometer insensitive to the IR differential light-shift inhomogeneities, such that the ALS laser is no longer necessary. We checked that the two interferometers (symmetrical or usual Ramsey-Raman with ALS) are equivalent, observing the same contrast behavior for $P_{IR} = 0.5$ W.

In Fig. 7 are summarized all the extracted decay rates plotted versus the IR power. Though the contrast decays were found for some measurements to deviate from pure exponential decays (especially at small IR power and for the waist closer to the atoms), we chose to quantify the loss of contrast by the rate obtained from an exponential decay fit in order to compare the results with calculations explained in the forthcoming section. We observe that the decay rates increase with the P_{IR} and with the distance between the IR waist and the atoms. Remarkably, the decay rates extrapolated at $P_{IR} = 0$ W are not null but reach similar values of about 0.4 /s for different positions.

As a complementary analysis, we measure the decay rates of a completely symmetric interferometer, that not only exchanges internal but also external states during the interferometer. This is realized using a spin-echo sequence [34] with a Raman π pulse inserted in the middle of the free evolution time of a Ramsey-Raman interferometer. This interferometer configuration is no longer sensitive to the Bloch

frequency and thus to the difference in the frequency between the Raman lasers. A phase shift can be applied between the two last pulses, enabling us to scan the phase and measure the contrast. We observe for this interferometer decay rates that are independent from the IR power: a plateau equal to 0.4/s, depicted by the green stars of Fig. 7. This confirms that the (partially) symmetric Ramsey-Raman interferometer suffers from an additional source of contrast loss, independent not only of the IR power but more generally of any inhomogeneity in the trapping potential.

B. Dephasing inhomogeneity

Different processes can lead to such contrast decays: decoherence or dephasing inhomogeneities. Most decoherence processes, such as Landau-Zener tunneling, parametrical heating, and spontaneous emission due to the trapping lasers, are common with the MW Ramsey interferometer. Spontaneous emission from the Raman lasers leads to a negligible loss of contrast of 0.3% and is independent from T_R. Thus these effects cannot explain the contrast decay of the Ramsey-Raman interferometer. We examine now possible sources of dephasing inhomogeneities, due to longitudinal or transverse confinement.

1. Longitudinal effects

The atoms being distributed along 4000 wells due to the initial cloud size, any force gradient along this cloud would cause a spread of the Bloch frequencies. The effect of the gravity gradient of about 3×10^{-7} g/m is clearly negligible. The effect of the IR laser is calculated to be a 15-mHz/cm displacement with respect to the laser waist for $P_{IR} = 0.5$ W. The spread over the 1-mm cloud is thus 1.5 mHz and induced a negligible contribution to the contrast decay rate. The lattice beam waist being much larger (~ 1 mm), similar effects are even weaker.

2. Transverse effects

For $P_{IR} = 0.5$ W, the depth of the IR trap is around 1.6 μK, when the atom's temperature at the end of the molasses phase is around 2 μK. The atoms will thus occupy all possible transverse states. When displacing the atoms from lattice site to lattice site, the shape of the potential changes and so does the energy of these transverse levels, from a different amount for each level. In the following, we will make the assumption that during the Raman pulses, atoms do not change of transverse state number n. The atom displacement being much smaller than the Rayleigh length, the initial n state and final n' are nearly orthogonal if $n \neq n'$.

To calculate how the different energy levels are shifted, we consider the Gaussian shape of the potential and follow a semiclassical approach. We calculate the density of states and the number of states having an energy lower than a given value E, $g(E)$ and $N(E)$, using equations from [35,36],

$$g(E) = \left(\frac{m_a}{2\pi\hbar^2}\right)^{n/2} \int_{U_{IR}(r)<E} \frac{[E - U_{IR}(r)]^{n/2-1}}{\Gamma(n/2)} dr^n, \quad (5)$$

$$N(E) = \frac{\pi^{n/2}}{h^n \Gamma(1+n/2)} \int_{U_{IR}(r)<E} \{2m_a[E-U_{IR}(r)]\}^{\frac{n}{2}} dr^n, \quad (6)$$

where $\Gamma(x)$ is the Riemann gamma function and n the number of dimensions of the integral. $g(E)$ and $N(E)$ are linked by the relation

$$N(E) = \int_{-U_{IR}}^{E} g(\epsilon) d\epsilon. \qquad (7)$$

Considering the problem as two dimensional, the equations are

$$g(E) = \frac{m_a}{2\pi\hbar^2} \iint_{U_{IR}(r)<E} dr^2 = \frac{m_a}{\hbar^2} \int_{U_{IR}(r)<E} r\, dr. \qquad (8)$$

The condition $U_{IR}(r) < E$ is equivalent to

$$r < \sqrt{\frac{-w_{IR}(z)^2}{2} \ln\left(\frac{E}{U_0(z)}\right)}, \qquad (9)$$

where $U_0(z)$ corresponds to the IR depth at the center of the beam. The quantities $g(E,z)$ and $N(E,z)$ are calculable analytically:

$$g(E,z) = \frac{-w_{IR}(z)^2}{4} \frac{m_a}{\hbar^2} \ln\left(\frac{E}{U_0(z)}\right), \qquad (10)$$

$$N(E,z) = \frac{m_a w_{IR}^2(z)}{4\hbar^2} \left[E - U_0(z) - E \ln\left(\frac{E}{U_0(z)}\right)\right], \quad (11)$$

and E varies between $U_0(z)$ and 0.

The total number of transverse states N_{tot} is given by $N(0,z)$. For $P_{IR} = 0.5$ W, $N_{tot} \sim 2 \times 10^6$, which validates the semiclassical approach. We numerically invert $N(E,z)$ in order to deduce $E(N,z)$. Calculating $E(N,z)$ and $E(N,z + \Delta m \lambda_l/2)$, we can deduce the energy shift of each level $\Delta E(N,z,\Delta m)$.

Having only in between 1 and 10 atoms per lattice site, the atomic density is too small for thermalization to play a role. We thus use a Boltzmann distribution f_B with a temperature $T_{at} = 2\,\mu$K, truncated at $E = 0$:

$$f_B(E) = \exp\left(\frac{-E - U_0(z)}{k_B T_{at}}\right). \qquad (12)$$

The mean energy shift is given by

$$\overline{\Delta E}(z,\Delta m) = A \int_0^{N_{tot}} \Delta E(N,z,\Delta m) f_B(E(N,z)) dN, \quad (13)$$

where A is a normalization constant: $A^{-1} = \int_0^{N_{tot}} f_B(E(N,z)) dN$. For $z \sim 2$ cm, $P_{IR} = 0.5$ W and $\Delta m = 6$, we find $\overline{\Delta E} \sim h \times 153$ mHz. The standard deviation of the energy shift is given by $\sigma_{\Delta E}(z,\Delta m)$, where

$$\sigma_{\Delta E}^2(z,\Delta m) = A \int_0^{N_{tot}} [\Delta E(N,z,\Delta m) - \overline{\Delta E}(z,\Delta m)]^2$$
$$\times f_B(E(N,z)) dN. \qquad (14)$$

Using the same parameters, we find $\sigma_{\Delta E} \sim h \times 122$ mHz, comparable to the mean energy shift, which indicates a rather large dispersion. We then simulate the interferometer fringe pattern by averaging the transition probability over the energy distribution $\Delta E(N)$ for various free precession times T_R, laser power P_{IR}, and waist-atoms distance z. We extract from the calculation of the contrast versus the free evolution time a decay rate by fitting the calculated data with an exponential

decay law. We determine the decay rates at three different positions: $z = -2$, $+1$, and 0.2 cm. We add to these decay rates a constant offset of 0.4/s, corresponding to the observed plateau of Fig. 7. For comparison with experimental data, we plot these calculated decay rates on Fig. 7 as black, red, and blue curves. We find a fair agreement with our measurements, which indicates that the dephasing due to the transverse spread of the dipole force can contribute significantly to the contrast loss when the atoms are not located at the IR waist.

C. Lattice laser effect

Our calculations do not take into account the effect of the lattice laser, when the measurements suggest that increasing the lattice depth increases contrast loss (cf. Fig. 6). We take advantage of the weak dependence of the Raman coupling on the $\Delta m = 6$ transition around its optimal value at 1.8 E_R to perform contrast decay measurements for different lattice depths in the range 1.2–2.2 E_R, keeping the IR laser power constant at 1 W. Figure 8 shows that the decay rates linearly increase with the depth in this range, though with slopes that are significantly different for the two kinds of interferometers. In the case of the Ramsey-Raman interferometer, the rate (displayed as red circles) varies by a factor of 2 in the range of depth explored here. For variations of the depth of about $\pm10\%$ around 1.8 E_R, which correspond to our estimate of the typical fluctuations during the measurements of Fig. 7, the decay rate can change by up to 0.3/s. This explains to a significant extent the dispersion we observe on these measurements for a given set of parameters. Moreover, the blue triangles of Fig. 8 indicate that the additional decay that constitutes the plateau is linked to the lattice depth, though we currently have no explanation for this effect. It is also consistent with the dispersion of the green stars on Fig. 7.
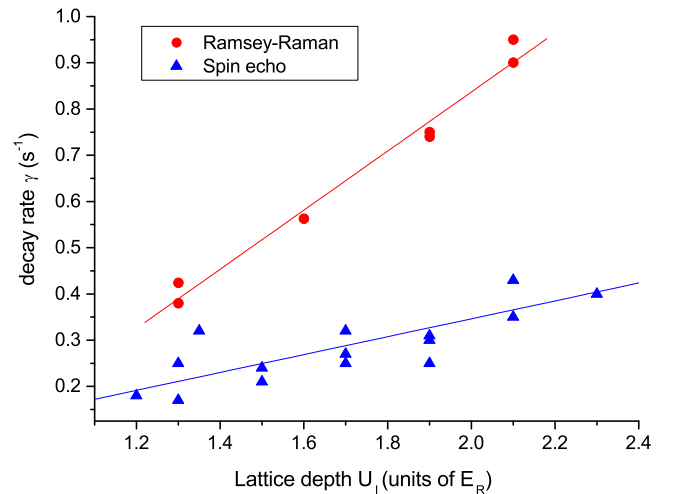

FIG. 8. (Color online) Interferometer contrast decay versus U_l. Red circles: Ramsey-Raman interferometer, blue triangles: spin-echo interferometer. Measurements were performed for $\Delta m = +6$ transition, for $P_{IR} = 1$ W, the IR waist on the atoms. Red and blue curves are linear fits to the data.

Our calculation does not allow a simple way to include the effect of the lattice laser, as the total potential is not separable and transverse and longitudinal directions are coupled.

VI. CONCLUSION

We have presented here a measurement of the Bloch frequency using a Ramsey-Raman interferometer scheme with atoms trapped in a 1D vertical lattice. Our apparatus allows for the measurement of the Bloch frequency with a relative sensitivity of 3.9×10^{-6} at 1 s for an IR waist 2 cm away from the atoms. Even though this sensitivity is not competitive with free-falling gravimeters reaching relative sensitivities of $\sim 5 \times 10^{-9}$ at 1 s [3,4], this experiment is at the state of the art when compared with another trapped configurations [25] where a relative sensitivity of 1.5×10^{-6} at 1 s was reached. Our sensitivity is limited on one hand by vibration noise and trapping laser noise, which could both be reduced using antivibration platforms, and on the other hand by the detection noise.

A significant influence of the IR laser power onto the value of ν_B has been observed, which indicates an offset of the atom position with respect to the laser waist. We could reduce this effect by moving the waist to the atom's position.

Finally, a study of the contrast decay as a function of the IR laser parameters was performed. A simple model allows us to quantitatively reproduce the measurements, provided that an additional source of loss is added, which we attribute to the lattice laser.

[1] A. Peters, K. Y. Chung, and S. Chu, Metrologia **38**, 25 (2001).

[2] M. Schmidt, A. Senger, M. Hauth, C. Freier, V. Schkolnik, and A. Peters, Gyroscopy and Navigation **2**, 170 (2011).

[3] Z.-K. Hu, B.-L. Sun, X.-C. Duan, M.-K. Zhou, L.-L. Chen, S. Zhan, Q.-Z. Zhang, and J. Luo, Phys. Rev. A **88**, 043610 (2013).

[4] P. Gillot, O. Francis, A. Landragin, F. Pereira Dos Santos, and S. Merlet, Metrologia **51**, L15 (2014).

[5] J. M. McGuirk, G. T. Foster, J. B. Fixler, M. J. Snadden, and M. A. Kasevich, Phys. Rev. A **65**, 033608 (2002).

[6] G. Lamporesi, A. Bertoldi, L. Cacciapuoti, M. Prevedelli, and G. M. Tino, Phys. Rev. Lett. **100**, 050801 (2008).

[7] T. L. Gustavson, A. Landragin, and M. A. Kasevich, Classical Quantum Gravity **17**, 2385 (2000).

[8] A. Gauguet, B. Canuel, T. Lévèque, W. Chaibi, and A. Landragin, Phys. Rev. A **80**, 063604 (2009).

[9] J. K. Stockton, K. Takase, and M. A. Kasevich, Phys. Rev. Lett. **107**, 133001 (2011).

[10] G. Tackmann, P. Berg, C. Schubert, S. Abend, M. Gilowski, W. Ertmer, and E. M. Rasel, New J. Phys. **14**, 015002 (2012).

[11] R. Bouchendira, P. Cladé, S. Guellati-Khélifa, F. Nez, and F. Biraben, Phys. Rev. Lett. **106**, 080801 (2011).

[12] B. Barrett, P.-A. Gominet, E. Cantin, L. Antoni-Micollier, A. Bertoldi, B. Battelier, P. Bouyer, J. Lautier, and A. Landragin, *Proceedings of the International School of Physics "Enrico Fermi"*, Atom Interferometry Vol. 188 (IOS Press, Amsterdam, 2014), pp. 493–555.

[13] Y. Bidel, O. Carraz, R. Charriere, M. Cadoret, N. Zahzam, and A. Bresson, Appl. Phys. Lett. **102**, 144107 (2013).

[14] R. Geiger, V. Ménoret, G. Stern, N. Zahzam, P. Cheinet, B. Battelier, A. Villing, F. Moron, M. Lours, Y. Bidel, A. Bresson, A. Landragin, and P. Bouyer, Nat. Commun. **2**, 474 (2011).

[15] Q. Bodart, S. Merlet, N. Malossi, F. Pereira dos Santos, P. Bouyer and A. Landragin, Appl. Phys. Lett. **96**, 134101 (2010).

[16] S. Merlet, L. Volodimer, M. Lours, and F. Pereira Dos Santos, Appl. Phys. B **117**, 749 (2014).

[17] J. Lautier, M. Lours, and A. Landragin, Rev. Sci. Instrum. **85**, 063114 (2014).

[18] G. Stern, B. Allard, M. Robert-de-Saint-Vincent, J.-P. Brantut, B. Battelier, T. Bourdel, and P. Bouyer, Appl. Opt. **49**, 3092 (2010).

[19] M. Andia, R. Jannin, F. Nez, F. Biraben, S. Guellati-Khélifa, and P. Cladé, Phys. Rev. A **88**, 031605 (2013).

[20] R. Charriere, M. Cadoret, N. Zahzam, Y. Bidel, and A. Bresson, Phys. Rev. A **85**, 013639 (2012).

[21] L. Huet, M. Ammar, E. Morvan, N. Sarazin, J.-P. Pocholle, J. Reichel, C. Guerlin, and S. Schwartz, Appl. Phys. Lett **100**, 121114 (2012).

[22] C. L. Garrido Alzar, W. Yan, and A. Landragin, *Research in Optical Sciences*, OSA Technical Digest (Optical Society of America, Washington, DC, 2012), Paper JT2A.10.

[23] F. Baumgärtner, R. J. Sewell, S. Eriksson, I. Llorente-Garcia, J. Dingjan, J. P. Cotter, and E. A. Hinds, Phys. Rev. Lett. **105**, 243003 (2010).

[24] Q. Beaufils, G. Tackmann, X. Wang, B. Pelle, S. Pelisson, P. Wolf, and F. Pereira dos Santos, Phys. Rev. Lett. **106**, 213002 (2011).

[25] M. G. Tarallo, T. Mazzoni, N. Poli, D. V. Sutyrin, X. Zhang, and G. M. Tino, Phys. Rev. Lett. **113**, 023005 (2014).

[26] G. Nenciu, Rev. Mod. Phys. **63**, 91 (1991).

[27] F. Bloch, Z. Phys. **52**, 555 (1929).

[28] R. Messina, S. Pélisson, M.-C. Angonin, and P. Wolf, Phys. Rev. A **83**, 052111 (2011).

[29] P. Wolf, P. Lemonde, A. Lambrecht, S. Bize, A. Landragin, and A. Clairon, Phys. Rev. A **75**, 063608 (2007).

[30] B. Pelle, A. Hilico, G. Tackmann, Q. Beaufils, and F. Pereira dos Santos, Phys. Rev. A **87**, 023601 (2013).

[31] M.-K. Zhou, B. Pelle, A. Hilico, and F. Pereira dos Santos, Phys. Rev. A **88**, 013604 (2013).

[32] R. Holzwarth, A. Yu Nevsky, M. Zimmermann, Th. Udem, T. W. Hänsch, J. von Zanthier, H. Walther, J. C. Knight, W. J. Wadsworth, P. ST. J. Russell, M. N. Skvortsov, and S. N. Bagayev, Appl. Phys. B **73**, 269 (2001).

[33] S. Pélisson, R. Messina, M.-C. Angonin, and P. Wolf, Phys. Rev. A **86**, 013614 (2012).

[34] M.-F. Andersen, A. Kaplan, and N. Davidson, Phys. Rev. Lett. **90**, 023001 (2003).

[35] P. Cvitanović, R. Artus, R. Mainieri, G. Tanner, and G. Vattay, *Chaos: Classical and Quantum* (Niels Bohr Institute, Copenhagen, 2012).

[36] M. V. Berry and K. E. Mount, Rep. Prog. Phys. **35**, 315 (1972).